Design and Characterization of 1.3-μm AlGaInAs–InP Multiple-Quantum-Well Lasers

Sandra R. Selmic, *Member, IEEE*, Tso-Min Chou, *Member, IEEE*, JiehPing Sih, Jay B. Kirk, Art Mantie, Jerome K. Butler, *Fellow, IEEE*, David Bour, *Fellow, IEEE*, and Gary A. Evans, *Fellow, IEEE*

***Abstract*—A comprehensive design method for long wavelength strained quantum-well lasers is applied to design uncooled multiple-quantum-well AlGaInAs–InP 1.3-μm lasers for communication systems. The method includes multiband effective mass theory and electromagnetic waveguide theory. The resulting AlGaInAs–InP laser has a threshold current of 12.5 mA at 25 °C, with a slope efficiency of 0.43 W/A, at 77 K orgreater characteristic temperature, a 38° perpendicular far-field beam divergence, and will operate at temperatures in excess of 100 °C.**

***Index Terms*—Optical waveguide theory, quantum theory, quantum-well lasers, ridge waveguides, semiconductor lasers.**

I. Introduction

OPTICAL-FIBER dispersion and loss are minimal at wavelengths near 1.3 and 1.55 μm, so semiconductor lasers emitting at these wavelengths are important light sources for optical networks. A goal for many applications is highly efficient uncooled semiconductor lasers, which can be achieved using $Al_xGa_yIn_{1-x-y}As$–InP [1]–[4] instead of the conventional Ga_x–In_{1-x}–As_y–P_{1-y}–In–P material system. This material system reduces carrier leakage from the quantum-well region (where carriers recombine to produce photons) compared to the conventional In–Ga–As–P material system under high temperature operation [1]. The reduced carrier leakage results from $Al_xGa_yIn_{1-x-y}As$–InP having a larger conduction band offset ($\Delta E_c = 0.72\Delta E_g$) at the heterojunctions compared to the smaller conduction band offset ($\Delta E_c = 0.4\Delta E_g$) of Ga_x–In_{1-x}–As_y–P_{1-y}–In–P. This is very significant because the effective mass of electrons in the conduction band is much less than the effective mass of holes in the valence band. As a result, it is much more important to provide a strong barrier to electrons in the conduction band (instead of a strong barrier to holes in the valence band) to prevent carrier leakage at high temperatures.

In this paper we present a complete design procedure for uncooled strained multiple-quantum-well ridge waveguide AlGaInAs–InP lasers emitting at a wavelength of 1.3 μm and compare the resulting fabricated devices with the theoretical predictions. To reduce the transparency current and the carrier density dependent loss due to the intervalence-band absorption, compressively strained-layer quantum-wells are chosen for the active layer.

In Section II, we present a theoretical model for both the quantum-well optical gain and the optical waveguide structure. In Section III we describe a complete design and optimization of the laser structure. In Section IV we present and discuss experimental results on AlGaInAs–InP lasers fabricated to this design.

II. Theory

A. Energy Levels in the Conduction and Valence Band

Because of the semiparabolic band nature for the conduction band, the single-band effective mass equation is used for finding the discrete energy levels inside the conduction band [5]

$$-\frac{\hbar^2}{2m_c^*}\nabla^2\Psi + V_c\Psi = E_c\Psi \tag{1}$$

where

ψ envelope function;
$\hbar$ Planck's constant divided by 2π;
m_c^* effective mass in the conduction band;
V_c conduction band potential;
E_c electron energy level in the conduction band.

For the energy band semiconductor structure shown in Fig. 1, the conduction band potential for a strained quantum-well is

$$V_c = \begin{cases} \frac{2}{3}\,\delta_h, & \text{quantum-well} \\ \Delta V_c^b, & \text{barrier layer} \\ \Delta V_c^c, & \text{cladding layer} \end{cases} \tag{2}$$

where δ_h is the hydrostatic potential, and ΔV_c^b and ΔV_c^c are conduction band offsets for the barrier and cladding layers, respectively. The hydrostatic potential is defined as

$$\delta_h = 2a\left(1 - \frac{C_{12}}{C_{11}}\right)\varepsilon \tag{3}$$

where

a hydrostatic deformation potential;
C_{11} and C_{12} elastic stiffness constants;
$\varepsilon = (a_b - a_q)/a_b$ strain constant, where a_q and a_b are lattice constants of the barrier and quantum-well layers, respectively.

Manuscript received October 10, 2000; revised June 29, 2001. This work was supported in part by the Advanced Technology Program of the Texas Higher Education Coordinating Board.

S. R. Selmic, T.-M. Chou, J. Sih, J. B. Kirk, J. K. Butler, and G. A. Evans are with the Department of Electrical Engineering, School of Engineering and Applied Science, Southern Methodist University, Dallas, TX 75275-0338 USA.

A. Mantie is with Laser Diode, Inc., Edison, NJ 08820 USA.

D. Bour is with Agilent, Palo Alto, CA 94304 USA.

Publisher Item Identifier S 1077-260X(01)08011-X.

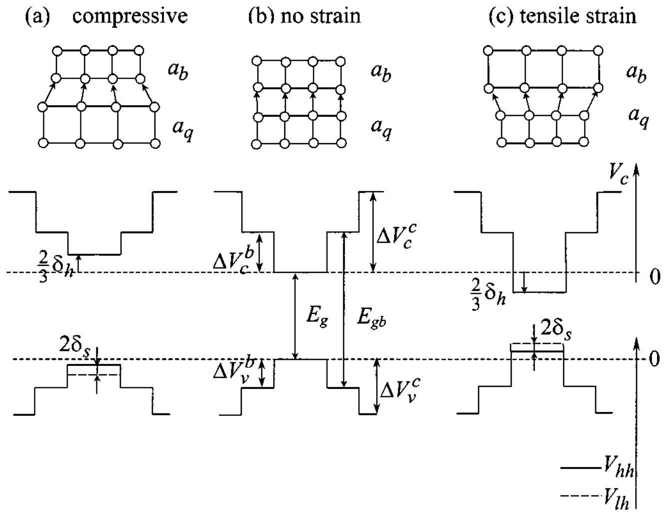

Fig. 1. The conduction V_c and valence V_{hh}, V_{lh} potentials for a semiconductor structure with quantum-well, barrier, and cladding layers. The barrier and the cladding are lattice matched materials. (a) Compressive strain between the quantum well and barrier. (b) No strain. (c) Tensile strain. Notation: ΔV_c^b, ΔV_v^b are the conduction and valence band offset for the barrier layer, ΔV_c^c, ΔV_v^c are the conduction and valence band offset for the cladding layer, a_q, a_b are the lattice constants for the quantum-well and barrier layers, δ_h is the hydrostatic potential, and δ_s is the shear potential.

Since the valence band structure in the quantum well is not parabolic, the multiband effective mass theory is used, giving coupled differential equations for heavy and light holes [6]. We can solve the resulting Kohn–Luttinger Hamiltonian [7] in order to get the envelope functions and energy levels in the heavy hole and light hole valance energy bands. The Schrödinger equation with the Kohn–Luttinger Hamiltonian for heavy and light holes is

$$\hat{H}\Psi = \begin{bmatrix} H & M & N & 0 \\ M^* & L & 0 & N \\ N^* & 0 & L & -M \\ 0 & N^* & -M^* & H \end{bmatrix} \Psi = E_v \Psi \qquad (4)$$

where ψ is the envelope function and E_v are the energy eigen values for electrons in heavy hole and light hole subbands. The elements H, L, M, and N in (4) are

$$H = -\frac{\hbar^2}{2m_0}\left[(k_x^2+k_y^2)(\gamma_1+\gamma_2) - (\gamma_1 - 2\gamma_2)\frac{\partial^2}{\partial z^2}\right] + V_{hh,\,lh} \qquad (5)$$

$$L = -\frac{\hbar^2}{2m_0}\left[(k_x^2+k_y^2)(\gamma_1-\gamma_2) - (\gamma_1 + 2\gamma_2)\frac{\partial^2}{\partial z^2}\right] + V_{hh,\,lh} \qquad (6)$$

$$M = i\,\frac{\sqrt{3}\,\hbar^2}{2m_0}(-k_y - ik_x)\gamma_3 \frac{\partial}{\partial z} \qquad (7)$$

$$N = -\frac{\sqrt{3}\,\hbar^2}{2m_0}\left[\gamma_2(k_x^2 - k_y^2) - 2i\gamma_3 k_x k_y\right] \qquad (8)$$

where

m_0	free electron mass;
γ_1, γ_2, γ_3	Luttinger parameters;
k_x and k_y	components of the transverse wavevector.

The heavy and light hole valence subband potential is

$$V_{hh} = \begin{cases} -\frac{1}{3}\,\delta_h + \delta_s, & \text{quantum well} \\ -\Delta V_v^b, & \text{barrier layer} \\ -\Delta V_v^c, & \text{cladding layer} \end{cases}$$

$$V_{lh} = \begin{cases} -\frac{1}{3}\,\delta_h - \delta_s, & \text{quantum well} \\ -\Delta V_v^b, & \text{barrier layer} \\ -\Delta V_v^c, & \text{cladding layer} \end{cases} \qquad (9)$$

where δ_s is the shear potential and ΔV_v^b and ΔV_v^c are the valence band offsets for the barrier and the cladding layer, respectively. The shear potential is defined as

$$\delta_s = 2b\left(1 + \frac{2C_{12}}{C_{11}}\right)\varepsilon \qquad (10)$$

where b is the shear deformation potential.

B. Optical Gain and Current Density

Knowledge of the optical material gain as a function of optical energy is required to find the appropriate material composition for the quantum wells of the laser. Due to the planar symmetry characteristic of the quantum-well wavefunction, the optical transition will depend on the polarization. The optical gain coefficient is a function of the photon energy and can be written as [5], [8]

$$G(E') = \frac{q^2|M_B|^2}{E'\varepsilon_0 m_0^2 c\hbar n_{\text{eff}} W} \cdot \sum_{i,\,j} \int_{E_g}^{E_{gb}} m_{r,\,ij} C_{ij} A_{ij} (f_c - f_v) L(E)\,\mathrm{d}E \qquad (11)$$

where

q	electron charge;
$\lvert M_B\rvert^2$	bulk momentum transition matrix element [9];
E'	photon energy;
ε_0	free-space permitivity;
c	vacuum speed of light;
n_{eff}	effective refractive index of the laser structure;
W	width of the quantum well;
i and j	conduction and valence band quantum numbers;
$m_{r,ij}$	spatially weighted reduced mass for transition;
$i \rightarrow j$, C_{ij}	spatial overlap factor between the states i and j;
$A_{i,j}$	angular anisotropy factor [5], [8];
f_c and f_v	electron quasi-Fermi functions in the conduction and valence band [10], respectively;
$L(E)$	Lorentzian lineshape function, commonly used to include the spectral broadening of each transition [5], [11].

Under high carrier concentrations common in quantum-well structures, the transition energy includes a many-body effect [12] known as bandgap renormalization [5]. At such high carrier concentrations, more vacant valence band states are available allowing the charges to redistribute for a stronger screening effect [8]. This screening will reduce the conduction electron energy and the transition energy between the conduction and valence bands [13]. As a result, the optical gain peak will move toward longer wavelengths with increased current injection. This mechanism is described with a Coulomb-hole self energy [14]

$$\Delta E_{CH} = -2E_R a_0 \mathrm{K} \ln\left[1 + \left(\frac{32\pi n W}{C_i \mathrm{K}^3 a_0}\right)^{1/2}\right] \tag{12}$$

where E_R, a_o, K, n, and W are the Rydberg energy, Bohr radius, inverse screening length, carrier density, and the width of the quantum well, respectively. C_i is the integration constant and the value is between one and four [13]. The transition energy with bandgap renormalization becomes

$$E_{ij} = E_c + |E_v| + E_g' = E_c + |E_v| + E_g + \Delta E_{CH} \tag{13}$$

where E_g is the energy gap in the quantum-well region.

The total current density through the device contains components due to both radiative and nonradiative recombination. The radiative recombination is dominated by spontaneous emission and the nonradiative recombination is dominated by Auger recombination [10]. The radiative part of the current density can be expressed as

$$\begin{aligned} J_{\text{radiative}} &= qWR(E') \\ &= qW\,\frac{16\pi^2 n_{\text{eff}} q^2 E\,|M_B|^2}{\varepsilon_0 m_0^2 c^3 \hbar^4 W} \\ &\quad \cdot \sum_{i,j} \int m_{r,ij} C_{ij}[f_c(1-f_v)]\,\mathrm{d}E \end{aligned} \tag{14}$$

where $R(E')$ is the spontaneous emission rate, and the nonradiative part can be expressed as

$$J_{\text{nonradiative}} = qWCnp^2 \tag{15}$$

where C is the Auger recombination coefficient.

C. Waveguide Theory, Confinement Factor, and Far-Field Distribution

The scalar form of the wave equation for TE modes in the dielectric waveguide with l layers is [15], [16]

$$\frac{\partial^2 \Phi_y(x)}{\partial x^2} + (k_0^2\varepsilon_i - \beta^2)\Phi_y(x) = 0, \qquad i = 1, 2 \cdots l \tag{16}$$

where

- ϕ_y electric field component;
- k_0 vacuum wavevector magnitude;
- ε_i dielectric constant of the ith dielectric layer;
- β electromagnetic wave propagation coefficient along the z axis (the coordinate system for waveguide mode analysis is different from the one introduced for the quantum-well analysis).

The wave equation for TM modes is similar to (16).

The fraction of the optical power of the mode contained in the active quantum-well layer is called the quantum-well confinement factor Γ_w and is defined in [17]

$$\Gamma_w = \frac{\int_{QW} \Phi_y^2(x)\,\mathrm{d}x}{\int_{-\infty}^{+\infty} \Phi_y^2(x)\,\mathrm{d}x}. \tag{17}$$

TABLE I
PARAMETERS FOR THE $\mathrm{Al}_x\mathrm{Ga}_y\mathrm{In}_{1-x-y}\mathrm{As}$ SYSTEM

	γ_1	γ_2	γ_3	C_{11}	C_{12}	a(eV)	b(eV)	m_c	a_0(Å)
AlAs	3.45	0.68	1.29	1.25	0.53	-5.64	-1.5	0.15	5.6611
GaAs	6.85	2.1	2.9	11.88	5.38	-9.7	-1.7	0.067	5.6533
InAs	20.4	8.3	9.1	8.329	4.526	-6.08	-1.8	0.023	6.0584

TABLE II
ENERGY GAP OF $\mathrm{Al}_x\mathrm{Ga}_y\mathrm{In}_{1-x-y}\mathrm{As}$

E_g =	0.526+1.516x (1-x-y =0.82)	2% compressive-strain
	0.572+1.517x (1-x-y =0.74)	1.5% compressive-strain
	0.638+1.532x (1-x-y =0.67)	1% compressive-strain
	0.75+1.548x (1-x-y =0.53)	lattice matched
	0.79+1.568x (1-x-y =0.38)	1% tensile-strain
	0.81+1.578x (1-x-y =0.307)	1.5% tensile-strain
	0.83+1.588x (1-x-y =0.225)	2% tensile-strain

The perpendicular far-field distribution of the semiconductor laser is the product of the Fourier transform of the near field ϕ_y and an obliquity factor $g(\theta)$ given in [18].

III. DESIGN OF THE 1.3-μm AlGaInAs MULTIPLE QUANTUM-WELL LASER

A. Material for Quantum Well, Barrier, and Cladding

The optical gain equations discussed above are solved using a transfer matrix method using a program called GAIN, which provides the energy levels, the wave functions, and the optical gain (including bandgap renormalization). A program called MODEIG [19] also uses a transfer matrix method to solve the electromagnetic wave equations discussed above. MODEIG provides a complete modal analysis resulting in the complex modal effective index, confinement factors for all layers, and the near- and far-fields. The modal gain ($\Gamma_{\mathrm{w}} G(E)$), the beam divergence, and the threshold current all have to be considered to properly design a laser structure.

Any quaternary parameter Q_{abcd} used in the gain calculations for the AlGaInAs material system is calculated by interpolation using

$$Q_{\mathrm{Al}_x\mathrm{Ga}_y\mathrm{In}_{1-x-y}\mathrm{As}} = (1-x-y)Q_{\mathrm{InAs}} + xQ_{\mathrm{AlAs}} + yQ_{\mathrm{GaAs}} \tag{18}$$

from the corresponding binary material parameters Q_{ij} which are listed in Table I [5], [10], [13], [20], [21].

The relation between energy gap and aluminum mole fraction x for the AlGaInAs material system [4], [22], [23] is summarized in Table II.

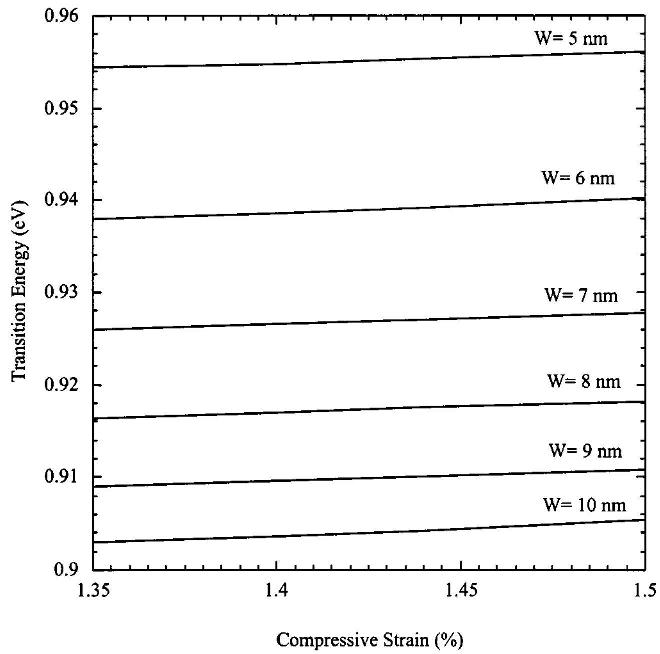

Fig. 2. Transition energy [see (13)] for the first energy level in the conduction and valence band versus compressive strain with quantum-well width as a parameter. The barrier energy gap is $E_{gb} = 1.16$ eV.

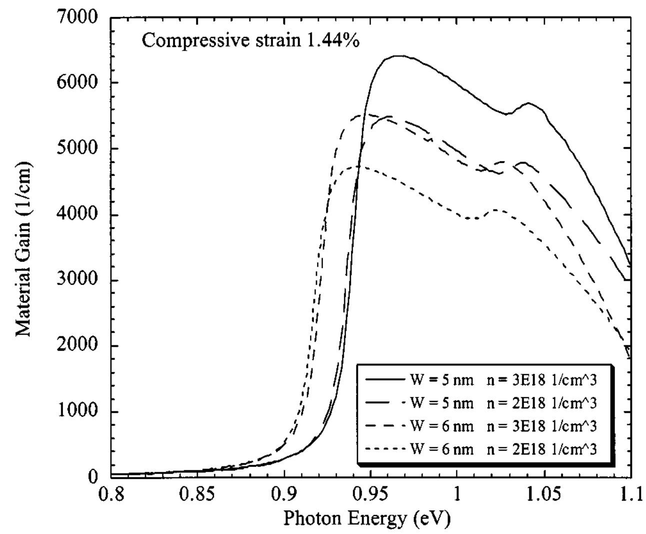

Fig. 3. Material gain versus optical energy for 1.44% compressive strain in a single quantum-well structure, for different quantum-well widths and carrier concentrations. The barrier energy gap is $E_{gb} = 1.16$ eV.

At a heterojunction in the $Al_xGa_yIn_{1-x-y}As$ material system, the band offset is mainly in the conduction band [4]

$$\Delta V_c = 0.72 \Delta E_g \tag{19}$$

where ΔE_g is the difference between the bandgaps at the heterojunction. The nonradiative recombination current is smaller than the radiative recombination current in InGaAsP lasers at room temperature [1], but must be included. After reviewing previous studies [8], [24]–[27], we choose the Auger coefficients to be $3.5 \cdot 10^{-30}$ cm^6 s^{-1} and $1.5 \cdot 10^{-29}$ cm^6 s^{-1} for 25 °C and 85 °C, respectively.

In order to find the right material composition of the quantum well for lasing at 1.3 μm, we start with the simple strained quantum-well structure shown in Fig. 1. For the inner cladding layer we choose $Al_{0.48}In_{0.52}As$ [4] to be lattice matched with the substrate InP. The energy gap of the barrier is important for selecting the proper material compositions of the quantum well. Since most of the effective optical transitions of III–V materials occurred at the Γ band center [5], we solve the diagonal elements of the Hamiltonian [see (5) and (6)] for $k_x = k_y = 0$. After several iterative applications of GAIN and MODEIG, we selected one of many possible solutions, $Al_{0.267}Ga_{0.203}In_{0.53}As$, which has an energy gap of 1.16 eV for the barrier layer.

The choice of composition of the quantum well is a complex procedure. We want the transition energy to correspond to a wavelength of 1.3 μm. However, the transition energy depends on the material composition of the quantum well, the material composition of the barriers, the width of the quantum well, and the strain of the quantum-well material. Fig. 2 shows the transition energy as a function of strain, with the quantum-well width as a parameter. The compressive strain is varied from 1.35% to 1.50%. For the target transition energy (13) around 0.947 eV, which corresponds to $\lambda = 1.3$ μm, we find an acceptable range for the strain of the single quantum-well material to be compressive from 1.4% to 1.45% with a well width between 5 and 6 nm if the quantum-well composition is about $Al_{0.16}Ga_{0.10}In_{0.74}As$.

Numerical calculations of the material gain for the TE mode for the single QW structure with 1.44% of compressive strain and for the quantum-well composition of $Al_{0.16}Ga_{0.10}In_{0.74}As$ are presented in Fig. 3 for different well widths and carrier concentrations. With a proper choice of the quantum-well width, a peak energy at 1.3 μm can be achieved.

B. Structure Optimization

After the analysis of the single quantum-well structure (Fig. 1) and choice of the compositions for the quantum well ($Al_{0.16}$–$Ga_{0.10}$–$In_{0.74}$–As), barrier ($Al_{0.267}$–$Ga_{0.203}$–$In_{0.53}$–As) and cladding ($Al_{0.48}$–$In_{0.52}$–As) regions for a peak energy close to 1.3 μm we proceed further with the design of the AlGaInAs laser.

A widely accepted logarithmic relationship between the modal gain $G_M(J)$ and current density J for quantum-well lasers is [28]

$$G_M(J) = \Gamma_w \cdot G(J) = \Gamma_w \cdot G_0 \left[\ln \left(\frac{J}{J_0} \right) + 1 \right]$$
$$= G_{0\text{modal}} \left[\ln \left(\frac{J}{J_0} \right) + 1 \right] \tag{20}$$

where G_0 and J_0 are the coefficients that are material and QW width-dependent. Equation (20) is very useful for the estimation of the optimum number of quantum wells and the resulting transparency current density. For the chosen single-quantum-well structure, the numerical results and the G_0–J_0 approximation (20) are both presented in Fig. 4, showing excellent agreement.

The optimum operating point for a single quantum well can be obtained from curves similar to Fig. 4 by finding the intersection of a line through the origin that is tangent to the G–J curve

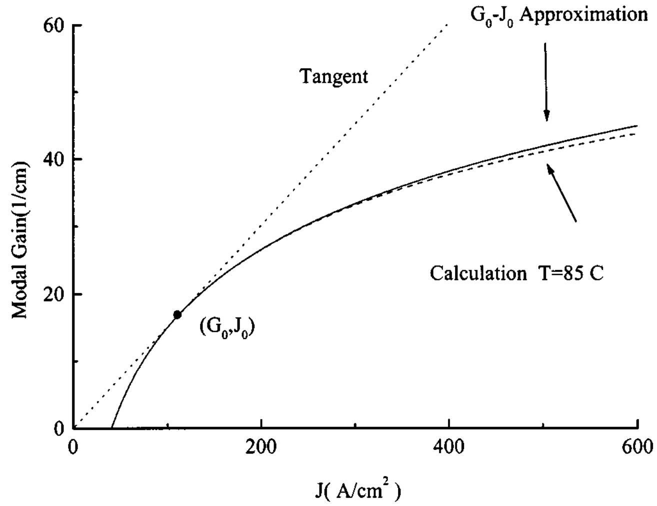

Fig. 4. Material gain versus optical energy for 1.44% compressive strain in a single quantum-well structure, for different quantum-well widths and carrier concentrations. The barrier energy gap is $E_{gb} = 1.16$ eV.

TABLE III
THE OPTIMUM NUMBER OF QUANTUM WELLS IN A COMPRESSIVELY STRAINED LASER STRUCTURE FOR DIFFERENT CAVITY LENGTHS AND OPERATIONAL TEMPERATURES

L	25^{o} C	65^{o} C	85^{o} C
250 μm	3 wells	4 wells	4 wells
300 μm	3 wells	4 wells	4 wells
500 μm	2 wells	2 wells	3 wells
700 μm	2 wells	2 wells	2 wells
1000 μm	2 wells	2 wells	2 wells

[28]. By calculating the G–J curve at the highest expected operating temperature, we can find the optimum gain per quantum well. We can then divide the total required threshold gain G_{th} by the optimum gain per quantum well G_0 and obtain the optimum number of quantum wells (Table III). The required gain at threshold is

$$G_{th} = \alpha_{\text{int}} + \frac{1}{2L} \ln \frac{1}{R_1 R_2} \tag{21}$$

where

α_{int} internal loss;
L cavity length;
R_1 and R_2 facet reflectivities.

Our design considerations suggest we use four 5-nm $Al_{0.16}Ga_{0.11}In_{0.73}As$ quantum wells separated by 10-nm $Al_{0.267}Ga_{0.203}In_{0.53}As$ barriers. Factoring in some uncertainty for the parameters used in the theoretical calculations along with growth and fabrication variations and a conservative design philosophy, we choose to add an additional quantum well (bringing the total to five) to the optimum number to ensure that we will have sufficient gain at 85 °C. Our simulations show that adding an additional quantum well beyond the optimum number slightly increases the threshold currents near room temperature but allows operation at temperatures well above the design limit.

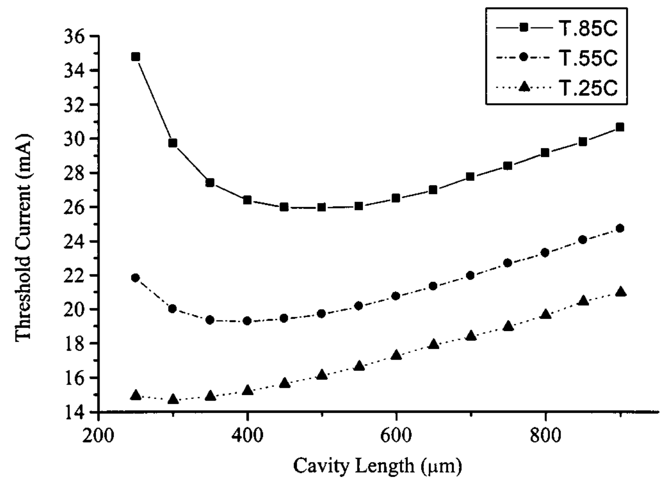

Fig. 5. Threshold current as a function of cavity length for different operating temperatures.

TABLE IV
THE CHARACTERISTIC TEMPERATURE OF THE AlGaInAs LASER FOR DIFFERENT CAVITY LENGTHS

L(μm)	T_0(K)
250	75.8
400	114.6
500	133.3
700	153.0
800	158.7
900	163.7

In high-speed optoelectronics, lasers with short cavity lengths, low threshold currents, and a wide temperature operation range are highly desirable. The choice of cavity length may be a tradeoff between optimum performance (low threshold current density, high T_0) and the number of laser die with acceptable performance produced per wafer. The relationship between the threshold current of the five-quantum-well structure and its cavity length for different temperatures is shown in Fig. 5. The cavity length for which the threshold current has a minimum value at the desired working temperature is called the optimum length and is around 500 μm at 85 °C.

The temperature variation of the threshold current of a laser is commonly described by a characteristic temperature defined by [10]

$$I_{th}(T) = I_0 \exp(T/T_0) \tag{22}$$

where I_o is a constant. The characteristic temperature depends on the cavity length (see Table IV). For the optimum length of 500 μm for the 85 °C working temperature, the characteristic temperature of the laser is predicted to be 133 K.facet reflectivities.

The epitaxial structure shown in Fig. 6 is composed of five quantum wells, four barriers, two graded-index (GRIN) layers, inner cladding layers, transition GRIN layers, one p-spacer, etch stop, and outer cladding. Thorough calculations and analysis with MODIEG allowed us to determine the optimum layer thicknesses. The variations of the confinement factor and

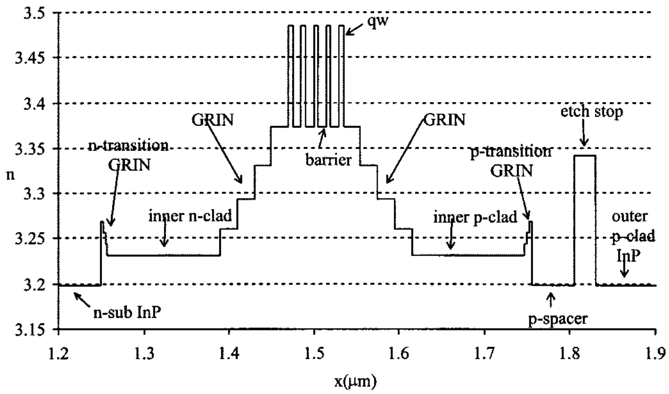

Fig. 6. Index of refraction along the epitaxial structure.

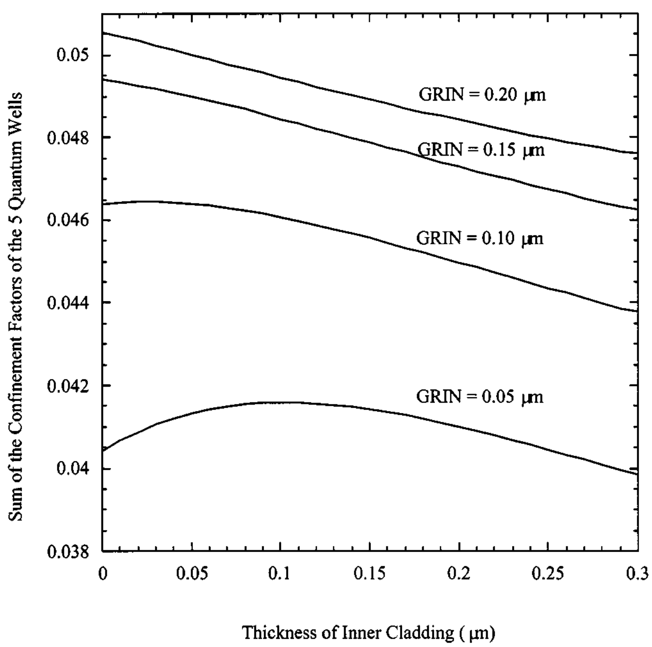

Fig. 7. Sum of the confinement factors of the five quantum wells versus thickness of inner cladding with GRIN layer thickness as a parameter.

far-field beam divergence as a function of GRIN layer thickness and inner cladding layer thicknesses are shown in Figs. 7 and 8. A compromise between a high confinement factor (which results in lower threshold currents) and a narrow far-field beam divergence (desirable for coupling light into an optical fiber) is required.

For ease of fabrication of a ridge-guide structure (shown in Fig. 9) to provide lateral optical confinement, an In–Ga–As–P etch stop layer with a 1.1-μm photoluminescence wavelength is inserted. Analysis shows that the thickness of the p-spacer and the etch stop layer affect the confinement factor and the far-field beam very little so this effect can be neglected in initial calculations. In order to guarantee that the laser operates in a single lateral mode, the lateral index step Δn must be carefully chosen [10] and we use an index step in the range of 0.005 to 0.02. Fig. 10 shows that the index step Δn can be adjusted by choosing the thickness of the p-spacer and GRIN layer.

In order to overcome the potential barrier to electron flow from the outer n-cladding (In–P) layer to the inner cladding ($Al_{0.48}$–$In_{0.52}$–As) layer, a thin, graded, and heavily n-doped

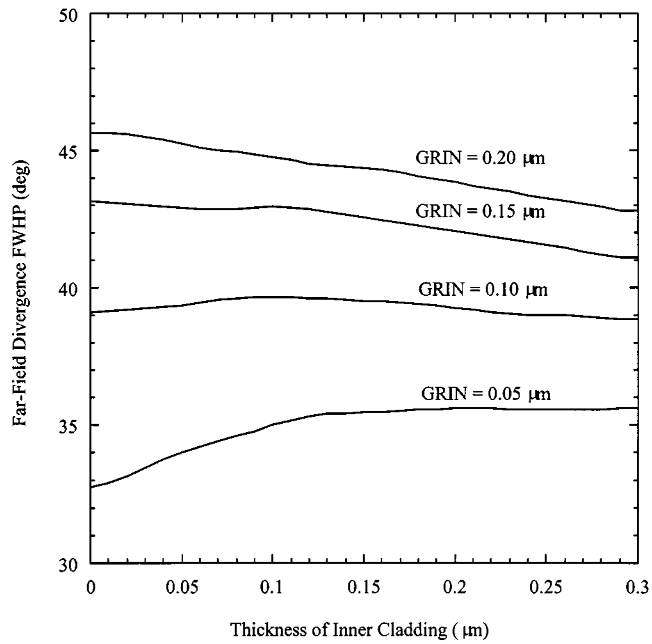

Fig. 8. Far-field beam divergence versus thickness of inner cladding with GRIN layer thickness as a parameter.

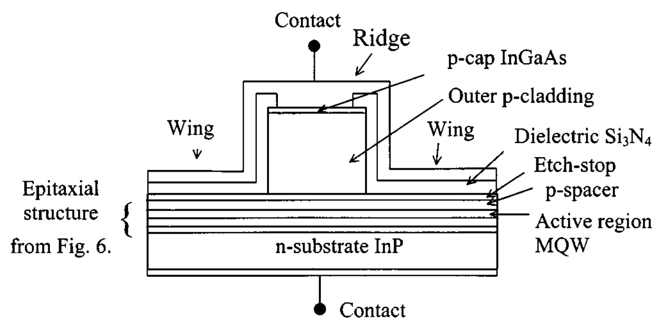

Fig. 9. Schematic representation of a ridge-waveguide laser.

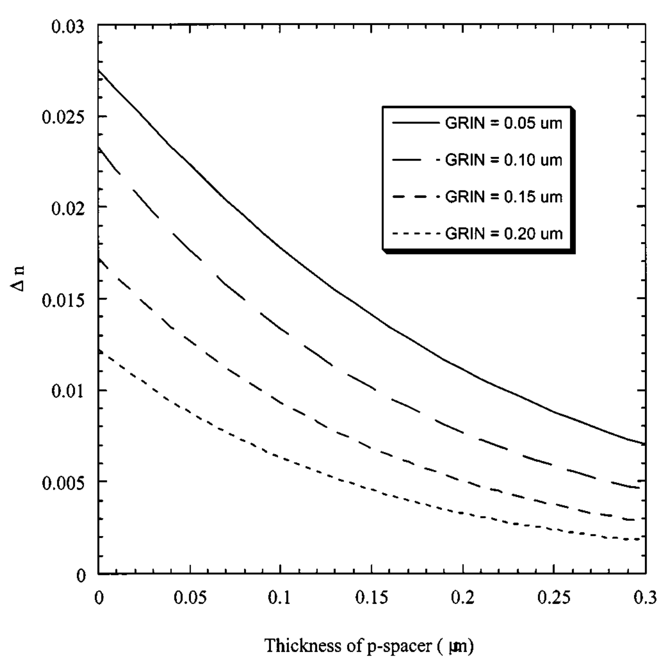

Fig. 10. The lateral index step as a function of the p-spacer thickness with GRIN-layer thickness as a parameter.

TABLE V
LIST OF THE LAYERS OF THE LASER STRUCTURE FROM FIG. 6

Layer	Composition	Thickness (μm)	Refractive index
n-substrate	InP	1.25	3.1987
n transition GRIN	$Al_{0.4128}Ga_{0.0672}In_{0.52}As$ to $Al_{0.48}In_{0.52}As$	0.01	3.2689-3.2310
inner n-cladding	$Al_{0.48}In_{0.52}As$	0.11	3.2310
n -GRIN	$Al_{0.48}In_{0.52}As$ to $Al_{0.267}Ga_{0.203}In_{0.53}As$	0.1	3.2310-3.3728
QW	$Al_{0.161}Ga_{0.102}In_{0.737}As$	0.005	3.4850
barrier	$Al_{0.267}Ga_{0.203}In_{0.53}As$	0.01	3.3728
QW	$Al_{0.161}Ga_{0.102}In_{0.737}As$	0.005	3.4850
barrier	$Al_{0.267}Ga_{0.203}In_{0.53}As$	0.01	3.3728
QW	$Al_{0.161}Ga_{0.102}In_{0.737}As$	0.005	3.4850
barrier	$Al_{0.267}Ga_{0.203}In_{0.53}As$	0.01	3.3728
QW	$Al_{0.161}Ga_{0.102}In_{0.737}As$	0.005	3.4850
barrier	$Al_{0.267}Ga_{0.203}In_{0.53}As$	0.01	3.3728
QW	$Al_{0.161}Ga_{0.102}In_{0.737}As$	0.005	3.4850
p -GRIN	$Al_{0.267}Ga_{0.203}In_{0.53}As$ to $Al_{0.48}In_{0.52}As$	0.1	3.3728-3.2310
inner p-cladding	$Al_{0.48}In_{0.52}As$	0.11	3.2310
p transition GRIN	$Al_{0.48}In_{0.52}As$ to $Al_{0.4128}Ga_{0.0672}In_{0.52}As$	0.01	3.2310-3.2689
p-spacer	InP	0.05	3.1987
Etch stop	InGaAsP	0.025	3.3414
Outer p-cladding	InP	1.25	3.1987
p-cap	InGaAs	0.2	3.0667

($Al_{0.48}$–$In_{0.52}$–As to In–P) transition layer is inserted between the outer n-cladding layer and inner cladding layer. A p-transition layer is also inserted between the outer and inner p-cladding layers in order to further reduce series resistance.

The thickness of each layer of our laser structure is given in Table V. The lateral index step Δn provided by the ridge guide is 0.0177.

IV. EXPERIMENTAL RESULTS FOR 1.3-μm AlGaInAs LASER

Al–Ga–In–As laser structures shown in Table V were grown by metal organic chemical vapor deposition by Epitaxial Products, Inc. (now International Quantum Epitaxial Products, Inc.). The continuous wave light-current characteristics for one of our AlGaInAs lasers at different operating temperatures are shown in Fig. 11. The theoretical agreement is within 6 to 10% for the threshold current (Fig. 12).

Fig. 12 shows theoretical predictions and curves for two different values of the ridge width (4 and 5 μm). The theoretical results indicate that the ridge width of the tested laser is closer to the value of 4.5 μm than to the 5-μm width of the ridge on the mask, due to undercutting during etching.

The characteristic temperature T_o (22) calculated from the experimental data for the 5-μm wide ridge waveguide laser (with a length of 250 μm) shown in Fig. 12 is 77 K, which is in agreement with theoretical calculations within 2%.

These ridge guide lasers have similar threshold currents, slope efficiencies, and characteristic temperatures reported for AlGaInAs 1.3-μm buried heterostructure lasers [3] but with lower threshold current densities ($\sim$1 kA/cm^2 versus $\sim$1.75 kA/cm^2 at room temperature). Although highly dependent on facet reflectivities, lengths, and far-field beam divergences, threshold current densities reported for other AlGaInAs ridge waveguides are in this same range (1.4 kA/cm^2 [29] and 2 kA/cm^2 [2]).

The experimental full-width at half-maximum beam divergences in perpendicular and lateral directions are 38° and 14° and are in agreement with theoretical calculations within 4% and 9%, respectively. Using a 4.5-μm value for the ridge gives a lateral far-field divergence within 3% of the experimental value.

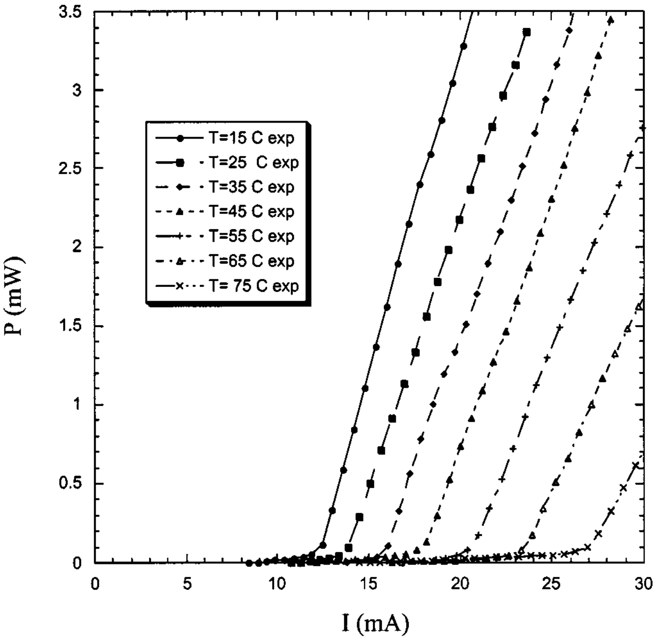

Fig. 11. Experimental light-current characteristics for a 1.3-μm AlGaInAs–InP laser. The ridge width, cavity length, and reflectivities are 5 μm, 250 μm, and 30%/70%, respectively.

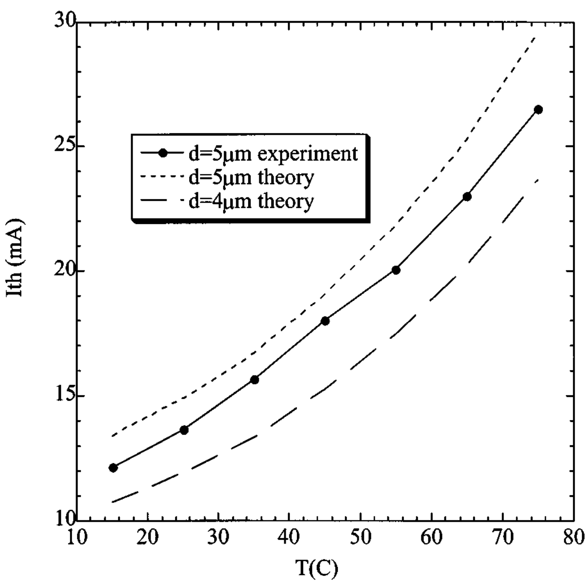

Fig. 12. Threshold current versus temperature for a 1.3-μm AlGaInAs–InP laser. Experimental and theoretical results ($L = 250$ μm).

The longitudinal-mode spectra of the AlGaInAs–InP laser are shown in Fig. 13. The mode spacing $\delta\lambda$ is given by $\delta\lambda = \lambda^2/(2Ln_g)$ [10] where λ is the lasing wavelength, L is the cavity length, and n_g is the group effective index of the laser mode. The measured mode spacing is about 0.97 nm, which is very close to the theoretical prediction (0.96 nm) for a 250-μm long laser.

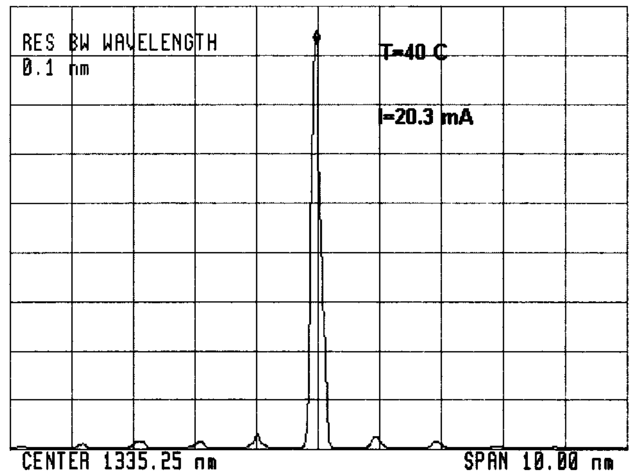

Fig. 13. Measured longitudinal-mode spectra for a 1.3-μm AlGaInAs laser. The center wavelength and mode spacing at 40 °C are 1335.2 nm and 0.97 nm, respectively.

V. Conclusion

In this paper, we have presented a comprehensive design method for long wavelength strained multiple quantum-well laser structures. We applied this method to 1.3-μm AlGaInAs–InP lasers for high-temperature operation. The strained multiple-quantum-well ridge-guide lasers grown and fabricated to this design had experimental characteristics within 10% or less of the theoretically predicted values. The threshold current was typically 12.5 mA for a length of 250 μm at room temperature and operation was achieved at temperatures in excess of 100 °C. The experimental far-field beam divergences were 38° perpendicular to the junction and 14° parallel to the junction.

References

[1] T. Higashi *et al.*, "Observation of reduced nonradiative current in 1.3-μm AlGaInAs-InP strained MQW lasers," *IEEE Photon. Technol. Lett.*, vol. 11, pp. 409–411, Apr. 1999.

[2] M. Yamada *et al.*, "High temperature characteristics of 1.3-μm InAsP-InAlGaAs ridge waveguide lasers," *IEEE Photon. Technol. Lett.*, vol. 11, pp. 164–166, Feb. 1999.

[3] K. Takemasa *et al.*, "1.3-μm AlGaInAs buried-heterostructure lasers," *IEEE Photon. Technol. Lett.*, vol. 11, pp. 949–951, Aug. 1999.

[4] C. E. Zah, R. Bhat, B. N. Pathak, F. Favire, W. Lin, M. C. Wang, N. C. Andreadakis, D. M. Hwang, M. A. Koza, T. P. Lee, Z. Wang, D. Darby, D. Flanders, and J. J. Hsieh, "High-performance uncooled 1.3-μm $Al_xGa_yIn_{1-x-y}As$/InP strained-layer quantum-well lasers for subscriber loop applications," *IEEE J. Quantum Electron.*, vol. QE-30, pp. 511–521, 1994.

[5] P. S. Zory, *Quantum Well Lasers*. San Diego, CA: Academic, 1993, pp. 58–150.

[6] D. A. Borido and L. J. Sham, "Effective masses of holes at GaAs-AlGaAs heterojunction," *Phys. Rev. B.*, vol. 31, pp. 888–892, 1985.

[7] S. L. Chuang, "Efficient band-structure calculations of strained quantum wells," *Phys. Rev. B*, vol. 43, no. 12, pp. 9649–9661, Apr. 1991.

[8] S. R. Chinn, P. S. Zory, and A. R. Reisinger, "A model for GRIN SCH-SQW diode lasers," *IEEE J. Quantum Electron.*, vol. 24, pp. 2191–2213, 1988.

[9] H. C. Casey, Jr. and F. Stern, "Concentration-dependent absorption and spontaneous emission of heavily doped GaAs," *J. Appl. Phys.*, vol. 47, no. 2, pp. 631–643, Feb. 1976.

[10] G. P. Agrawal and N. K. Dutta, *Semiconductor Lasers*. New York: Van Norstrand Reinhold, 1993, pp. 30–135.

[11] A. I. Kucharska and D. J. Robbins, "Lifetime broadening in GaAs-AlGaAs quantum well lasers," *IEEE. J. Quantum Electron.*, vol. 26, pp. 443–448, 1990.

[12] M. F. Periera, Jr., S. W. Koch, and W. W. Chow, "Effects of strain and Coulomb interaction on gain and refractive index in quantum-well lasers," *J. Optical Soc. Amer. B*, vol. 10, no. 5, pp. 765–773, 1993.

[13] W. W. Chow, S. W. Koch, and M. Sargent, III, *Semiconductor Laser Physics*. New York: Springer-Verlag, 1994, pp. 35–205.
[14] M. F. Pereira, Jr. and S. W. Koch, "Many-body effects in the spectra of strained quantum wells," *Appl. Phys. Lett.*, vol. 59, no. 23, pp. 2941–2943, 1991.
[15] D. Marcuse, *Theory of Dielectric Optical Waveguides*. New York: Academic, 1974, p. 9.
[16] H. Kressel and J. K. Butler, *Semiconductor Lasers and Heterojunction LEDs*. New York: Academic, 1977, p. 172.
[17] P. Bhattacharya, *Semiconductor Optoelectronic Devices*, NJ: Prentice-Hall, 1994.
[18] H. C. Casey, Jr. and M. B. Panish, *Heterostructure Lasers*. Orlando, FL: Academic, 1975, pt. A, p. 75.
[19] R. Smith and G. Mitchell, "Calculation of complex propagating modes in arbitrary, plane-layered, complex dielectric structures," Univ. Washington, Seattle, WA, EE Technical Rep. 206, Note: A PC version of MODEIG can be downloaded at http://www.seas.smu.edu/modeig/ along with the input files used to generate the designs used in this paper., Dec. 1977.
[20] C. G. Van de Walle, "Band lineups and deformational potentials in the model solid theory," *Phys. Rev. B*, vol. 39, no. 3, pp. 1871–1883, 1989.
[21] S. Adachi, "Material parameters of In_{1-x} Ga_x As_y P_{1-y} and related binaries," *J. Appl. Phys.*, vol. 53, no. 12, pp. 8775–8793, 1982.
[22] H. C. Casey, Jr. and M. B. Panish, *Heterostructure Lasers*. Orlando, FL: Academic, 1975, pt. B, pp. 45–46.
[23] T. Ishikawa and J. E. Bowers, "Band lineup and in-plane effective mass of InGaAsP or InGaAlAs on InP strained-layer quantum well," *IEEE J. Quantum Elect.*, vol. 30, pp. 562–570, 1994.
[24] R. I. Taylor, R. A. Abram, M. G. Burt, and C. Smith, "A detailed study of Auger recombination in 1.3 μm InGaAsP/InP quantum wells and quantum wires," *Semicon. Sci. Technol.*, vol. 5, pp. 90–104, 1990.
[25] L. A. Coldren and S. W. Corzine, *Diode Lasers and Photonic Integrated Circuits*. New York: Wiley, 1995, pp. 158–160.
[26] J. Minch, S. H. Park, T. Keating, and S. L. Chuang, "Theory and experiment of $In_{1-x}Ga_xAs_y$ P_{1-y} and $In_{1-x-y}Ga_x$ Al_yAs long-wavelength strained quantum-well lasers," *IEEE J. Quantum Electron.*, vol. 35, pp. 771–782, May 1999.
[27] M. Takeshima, "Effect of Auger recombination on laser operation in $Ga_{1-x}Al_x$As," *J. Appl. Phys.*, vol. 58, no. 10, pp. 3846–3850, Nov. 1985.
[28] P. W. McIlroy, A. Kurobe, and Y. Uematsu, "Analysis and application of theoretical gain curves to the design of multi-quantum-well lasers," *IEEE. J. Quantum Electron.*, vol. 21, pp. 1958–1963, 1985.
[29] T. R. Chen, P. C. Chen, J. Ungar, M. A. Newkirk, S. Oh, and N. Bar-Chaim, "Low-threshold and high-temperature operation of InGaAlAs–InP lasers," *IEEE Photon. Technol. Lett.*, vol. 9, pp. 17–18, Jan. 1997.

Sandra R. Selmic (M'96) was born in Belgrade, Yugoslavia, in 1971. She received the B.S. and M.S. degrees in electrical engineering from the University of Belgrade, Yugoslavia, in 1994 and 1997, respectively.

Since 1998, she has been a Ph.D. student and a Graduate Research Assistant at the Department of Electrical Engineering of Southern Methodist University, Dallas, TX. Her research interests include novel long-wavelength and high-power semiconductor lasers. Her other research interests are quantum effects in semiconductor microstructures and fiber-optic sensors. She has authored a total of 11 publications and conference presentations.

Ms. Selmic received the IEEE LEOS student paper award from the Dallas section for 1999 and the Graduate Student Research Award from Sigma Xi SMU in 2000.

Tso-Min Chou (S'92–M'95) was born in Taipei, Taiwan, on June 29, 1961. He graduated from the Tamkang University, Taipei, in 1988 and received the M.S. and the Ph.D. degrees from Southern Methodist University, Dallas, TX, in 1990 and 1996, respectively.

From 1996 to 2000, he worked at Southern Methodist University completing postdoctoral research. He currently works as Researcher at TriQuint Semiconductor Dallas, TX.

JiehPing Sih, photograph and biography not available at the time of publication.

Jay B. Kirk was born in Brewster, WA, in 1951. He received the A.S. degree in aircraft maintenance from Spokane Community College in 1971 and has an FAA airframe and powerplant license.

Until 1980, he worked for several companies in the aerospace industry. In 1980 he joined the Aerospace Corporation, El Segundo, CA, where he was involved with the fabrication of conventional cleaved-facet, integrated cavity, and DBR-surface-emitting semiconductor lasers. At TRW, Redondo Beach, CA, from 1981 to 1985, he constructed an MOCVD epitaxial growth system, various material characterization systems, and fabricated semiconductor lasers. He joined RCA Laboratories, Princeton, NJ, in 1985, where he constructed a submicron holographic grating fabrication system, developed wet and dry etching processes, and contributed to the development of DFB, DBR, and grating-surface-emitting semiconductor lasers. He has over 50 publications and one patent. Since 1993, he has been the Laboratory Manager for the Electrical Engineering Department at Southern Methodist University.

Mr. Kirk was awarded the David Sarnoff Outstanding Achievement Award, in 1987.

Art Mantie, photograph and biography not available at the time of publication.

Jerome K. Butler (F'90) received the B.S.E.E. degree from Louisiana Polytechnic Institute, Ruston, in 1960 and the M.S.E.E. and Ph.D. degrees from the University of Kansas, Lawrence, in 1962 and 1965, respectively.

From 1960 to 1965, he was a Research Assistant and held a CRES Fellowship at the Center for Research in Engineering Sciences, University of Kansas. He conducted research concerned with electromagnetic wave propagation and the optimization and synthesis techniques of antenna arrays. In 1965, he joined the faculty of the School of Engineering and Applied Science, Southern Methodist University, Dallas, TX, where he is now a University Distinguished Professor and past Chair of Electrical Engineering. His primary research areas include solid-state injection lasers, radiation and detection studies of lasers, communication and fiber-optic systems, integrated optics, the application of integrated optical circuits, and quantum electronics. In summers 1969–1992, he was a Staff Scientist, Sarnoff Corporation (formerly RCA Laboratories), Princeton, NJ. He has held consulting appointments with the Central Research Laboratory of Texas Instruments, Inc., the Geotechnical Corporation of Teledyne, Inc., Earl Cullum Associates, the University of California Los Alamos Scientific Laboratory, and Raytheon. He is a registered professional engineer in the State of Texas.

Dr. Butler was given the Southern Methodist University Sigma Xi Research Award, in 1977 . He was elected a Fellow of IEEE for "contributions to semiconductor lasers and the theory of radiation characteristics of optical waveguides." He is a member of Sigma Xi, Tau Beta Pi, and Eta Kappa Nu.

David Bour (S'84–M'85–SM'97–F'00) received the B.S. degree in physics from Massachsetts Institute of Technology, Cambridge, MA, in 1983 and the Ph.D. degree in electrical engineering from Cornell University, Ithica, NY, in 1987.

He is a Principal Scientist at the Communications and Optics Research Laboratory at Agilent Laboratories, Palo Alto, CA, where he is working on the epitaxial growth of semiconductor lasers by metal–organic chemical vapor deposition. From 1991 to 1999 he was a Principal Scientist in the Electronic Materials Laboratory of the Xerox Palo Alto Research Center, fabricating nitride blue laser diodes and phosphide red laser diodes for laser printing. Prior to this, at Sarnoff Corporation, he contributed to the development of InGaAs–AlGaAs materials for high power long-lived lasers near infarred wavelengths, used for pumping optical fiber amplifiers and for grating-surface-emitting laser arrays.

Gary A. Evans (S'74–M'75–SM'82–F'92) was born in Omak, WA. He received the B.S.E.E. degree from the University of Washington, Seattle, in 1970 and the M.S.E.E. and Ph.D. degrees in electrical engineering and physics from the California Institute of Technology (Caltech), Pasadena, in 1971 and 1975.

After a postdoctoral year at Caltech, he worked for R&D Associates, Marina Del Rey, CA, and was a Visiting Assistant Professor in the Electrical Engineering Department at the University of Washington (1977–1979). He has worked at the Aerospace Corporation, El Segundo, CA (1979–1981), TRW, Redondo Beach, CA (1981–1984), and RCA Laboratories (now Sarnoff Corporation), Princeton, NJ (1984–1992). In 1992, he joined Southern Methodist University, Dallas, TX, as a Professor in the Electrical Engineering Department. Since 1979, he has primarily worked on the design, growth, and fabrication of conventional cleaved facet and grating surface emitting semiconductor lasers. He has over 200 publications, five patents, and is a co-editor of the book *Surface Emitting Semiconductor Lasers*New York:Academic Press. He is a licensed professional engineer.

Dr. Evans was elected a Fellow of the IEEE for "contributions to the development, fabrication, and understanding of semiconductor lasers." He has served on numerous IEEE committees, is a past Chairman of the Princeton, NJ, and Dallas, TX Sections of the Lasers and Electro-Optics Society (LEOS), a past Chairman of the Santa Monica Bay Section of the IEEE, was an Associate Editor of the IEEE JOURNAL OF QUANTUM ELECTRONICS (1989–1995), was the Finance Chairman for the 1994 IEEE International Semiconductor Laser Conference, and was a Technical Program Vice Chair for the 1996 International Communications Conference.